Journal of Power Sources 190 (2009) 293–300

Contents lists available at ScienceDirect

Journal of Power Sources

journal homepage: www.elsevier.com/locate/jpowsour

Electrocatalysis of oxygen reduction on carbon-supported Pt–Co nanoparticles with low Pt content

F.H.B. Lima*, J.F.R. de Castro, L.G.R.A. Santos, E.A. Ticianelli

Instituto de Química de São Carlos, Universidade de São Paulo, CP 780, 13560-970 São Carlos, SP, Brazil

ARTICLE INFO

Article history:
Received 29 November 2008
Received in revised form 31 December 2008
Accepted 31 December 2008
Available online 14 January 2009

Keywords:
Pt–Co/C nanoparticles
Oxygen reduction
Alkaline fuel cell
Carbon-supported electrocatalyst

ABSTRACT

The oxygen reduction reaction (ORR) was investigated on carbon-supported Pt–Co nanoparticle electrocatalysts with low Pt content in alkaline electrolyte. High resolution transmission electron microscopy, *In situ* X-ray absorption spectroscopy, and X-ray diffraction analysis evidenced large structural differences of the Pt–Co particles depending on the route of the catalyst synthesis. It was demonstrated that although the Pt–Co materials contain low amounts of Pt, they show very good activities when the particles are formed by a Pt-rich shell and a Pt–Co core, which was obtained after submitting the electrocatalyst to a potential cycling in acid electrolyte. The high activity of this material was due to a major contribution from its higher surface area, as a result of the leaching of the Co atoms from the particle surface. Furthermore, its high activity was ascribed to a minor contribution from the electronic interaction of the Pt atoms, at the particle surface, and the Co atoms located in the beneath layer, lowering the Pt d-band center. As these electrocatalysts presented high activity for the ORR with low Pt content, the cost of the fuel cell cathodes could be lowered considerably.

1. Introduction

Carbon-supported platinum electrocatalysts usually show large surface area and high catalytic activity for the oxygen reduction reaction (ORR) both, in acid and alkaline media. Many works [1–3] have reported that some Pt-based alloy catalysts show higher activity than Pt-alone, and this has been ascribed to changes in the Pt–Pt bond distance and Pt electronegativity [4], electron density in the 5d Pt band [5], and surface oxide layers [6].

Some published papers [7–10] have shown that the catalytic activity of metals can be rationalized in terms of the energy of the d-band center (ε_d). The proposed model focuses on the shift of the d-band center, increasing or decreasing the reactivity of metal catalysts. This is based on a general principle ruling the formation of chemical bonds at a surface: strong bonding occurs if anti-bonding states are shifted up through the Fermi level (and become empty). The opposite occurs if anti-bonding states are shifted down through the Fermi level (and become filled). The variation of the d-band center has been theoretically demonstrated by surface segregated phases of a given metal on metal nanoparticles. It was seen that, for example, alloying Pt with Co [8] or taking Co as the host element and Pt atoms as the solute [7], there is a surface segregation of Pt. The calculations have shown a down-shift of the d-band center of Pt segregated on the surface of the Co nanoparticle. [8]. A down shift of the d-band center conducts to the formation of occupied anti-bonding orbitals and, as a consequence, for the case of the ORR, conducts to a weak Pt–OH and/or Pt–O^- adsorption strength.

Stamenkovic et al. [11] analyzed the activity towards the ORR of several Pt-3d-metal alloys. The plot of activity *vs.* d-band center showed a "volcano" dependency, with Pt–Co/C situated on the top of this curve. The activity enhancement of Pt–Co/C in relation to Pt/C was associated to a decrease of the Pt d-band center, lowering the adsorption strength of the adsorbed oxygenated species. This results in a lower Pt oxide coverage (from water activation) and/or faster electro-reduction of the oxygenated intermediates, enhancing the ORR kinetics. Similar observations were previously presented by Zhang et al. for a Pt-overlayer on different metal single-crystals [12].

In the present work, the oxygen reduction reaction (ORR) was studied in alkaline media on carbon-supported Pt and Pt–Co particles, which are one of the best materials for the ORR electrocatalysis, as demonstrated by the Ref. [11]. The metal particles were synthesized by two different manners and submitted to different temperatures of thermal treatment in H_2 atmosphere, aiming at preparing structures with segregated Pt atoms at the surface of the Co-rich cores. High resolution transmission electron microscopy and X-ray diffraction were employed to characterize the metal nanoparticle distribution on the carbon support and to estimate the size and crystallite structure of the catalyst metal clusters. *In situ* X-ray absorption near edge structure analysis was carried out to examine the electronic structure of Pt alloyed with the Co atoms.

* Corresponding author at: Av. Trabalhador Sãocarlense, 400, CP 780, CEP 13560-960, São Carlos, SP, Brazil. Tel.: +55 16 3373 8681; fax: +55 16 3373 9952.
E-mail address: fabiohbl@iqsc.usp.br (F.H.B. Lima).

0378-7753/$ – see front matter © 2009 Elsevier B.V. All rights reserved.
doi:10.1016/j.jpowsour.2008.12.128

The electrochemical techniques considered were cyclic voltammetry (CV) and steady state polarization, which were conducted by using the standard rotating disk electrode. The spectroscopic and the electrochemical results were compared in order to correlate the kinetics of the ORR with the electronic and structural properties of the catalysts.

2. Experimental

2.1. Synthesis of the Pt–Co/C nanoparticles

The electrocatalysts consisted of home-made 20 wt.% of Pt–Co dispersed on high surface area carbon (Vulcan XC-72, Cabot, 250 $m^2\ g^{-1}$), represented as Pt–Co/C, with atomic ratios (Pt:Co) of 1:3 and 1:5. The catalyst synthesis involved two different routes: (i) Borohydrid method (BM): the catalysts were prepared by chemical reduction of a solution of H_2PtCl_6 (Aldrich) and Co_2NO_3 (Merck) using $NaBH_4$. The reduction process was carried out at 60 °C by adding drops of a sodium borohydrid solution, in excess, into an aqueous slurry suspension, prepared in ultrasound for 10 min, and containing the carbon powder and the solubilized metal salts. The resulting powder was filtered, washed, and dried. (ii) Impregnation method (IM): the electrocatalysts were prepared by impregnating the high surface area carbon with an aqueous solution of H_2PtCl_6 and Co_2NO_3 under sonication for 10 min. The impregnated carbon was then dried by evaporation of the water in a petri plate at 80 °C. The resulting powders obtained by these two procedures were submitted to thermal treatments conducted in a tubular oven (MAITEC) under H_2 atmosphere at 200, 500 and 800 °C for 1 h. Similar approaches for catalyst preparations were published elsewhere [13,14]. In this work, the different electrocatalysts are designed by: Pt–Co/C, followed by the atomic ratio (1:3 or 1:5), synthesis route (IM or BM) and by the temperature of thermal treatment.

2.2. Catalyst characterization

The catalyst composition was first estimated by energy dispersive X-ray technique (EDX), using a digital scanning microscope (DSM 960 from Zeiss) with micro-analyzer Link Analytical QX 2000, using an electron beam of 63 kV. Structural information, as the catalyst dispersion and particle size on the carbon support, and relative composition of Pt and Co, was obtained by high resolution transmission electron microscopy (HRTEM) and *in situ* energy dispersive spectroscopy (EDS) using a JEM-3010 ARP microscope. The samples for the HRTEM analyses were prepared by dispersing the catalysts in ultrasound in ethanol. A drop of the resulting dispersion was placed onto the thin carbon films deposited on standard

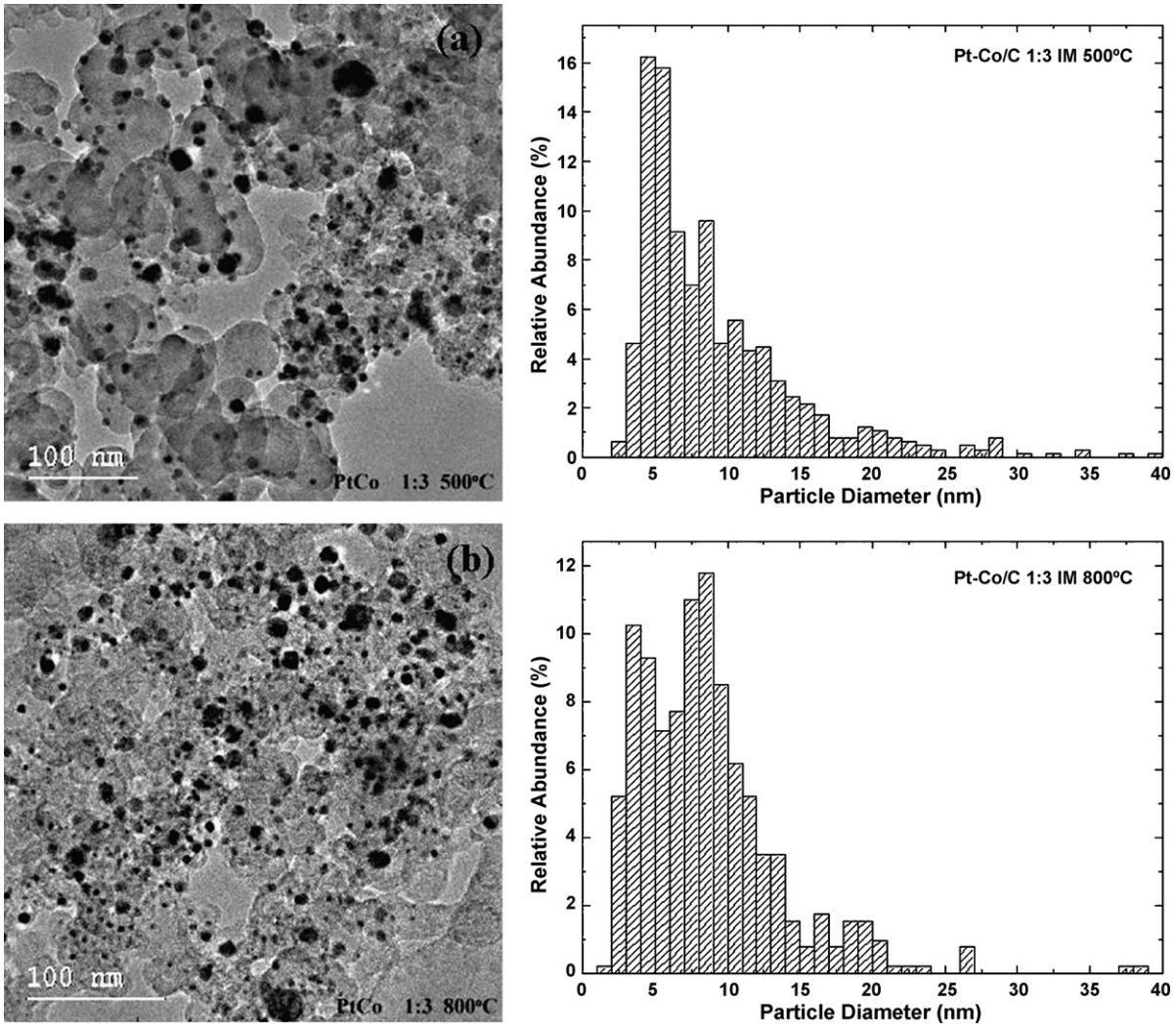

Fig. 1. TEM micrographs and particle size distribution histograms obtained for the Pt–Co/C 1:3 catalysts prepared by the Impregnation Method and treated at (a) 500 °C and (b) 800 °C, in hydrogen atmosphere.

HRTEM copper grids, and dried in air. The images were accquired by observing many different areas of the samples, in order to assess its average characteristics; at least five different areas, randomly chosen, were imaged under low magnification. The diameters of the catalyst particles were measured from the HRTEM images using Digital Micrograph software from GATAN. At least 500 nanoparticles of each sample were measured to build the size distribution histograms.

Physical properties such as lattice structure and the average crystallite size were investigated by X-ray diffraction (XRD) (RIGAKU, model RU200B) measurements carried out in the 2θ range from 20° up to 100° and using Cu K_α radiation (with a scan rate of 2° min^{-1}). The electronic features were studied by *in situ* X-ray absorption spectroscopy (XAS) in the X-ray absorption near edge structure (XANES) region, and it was performed at the Pt L_3 absorption edge, using a home-made spectroelectrochemical cell [15]. The working electrodes for the XAS measurements were pellets composed by the electrocatalysts agglutinated with Nafion® (*ca.* 30 wt.%) and containing 6.0 mg_{Pt} cm^{-2}. The counter electrode was formed with a Pt screen. This electrode was cut in the center, in order to allow the free passage of the X-ray beam. XAS experiments were made at 0.20 and 0.90 V *vs*. a reversible hydrogen electrode (RHE) after cycling the electrodes in the range defined by these potentials. Results presented here correspond to the average of at least two independent measurements.

The experiments were conducted at the D04-XAFS1 beam line in the Brazilian Synchrotron Light Source Laboratory (LNLS), Brazil. The data acquisition system comprised three ionization detectors (incidence I_0, transmitted I_t and reference I_r). The reference channel was employed primarily for internal calibration of the edge positions by using a pure foil of the metals. Nitrogen was used in the I_0, I_t and I_r chambers, and a Si(1 1 1) singlecrystal of third-order was used as monochromator. So, third-order harmonic contamination of the Si (1 1 1) monochromatic beam is expected to be negligible above 5 keV [16]. The computer program used for the analysis of the XAS data was the WinXAS package [17]. The data analysis was performed according to the procedures described in more detail in the literature [18,19]. Briefly, the XANES spectra were first corrected for the background absorption by fitting the pre-edge data (from −60 to −20 eV below the edge) to a linear formula, followed by extrapolation and subtraction form the data over the energy range of interested. Next, the spectra were calibrated for the edge position using the second derivative of the inflection point at the edge jump of the data from the reference channel. Finally, the spectra were normalized, taking as reference the inflection point of one of the EXAFS (extended X-ray absorption fine structure) oscillations.

A conventional one compartment electrochemical glass cell with a Luggin capillary was used in the electrochemical experiments. A large area platinized platinum screen served as the counter electrode and a Hg/HgO (KOH 1.0 mol L^{-1}) system was used as the

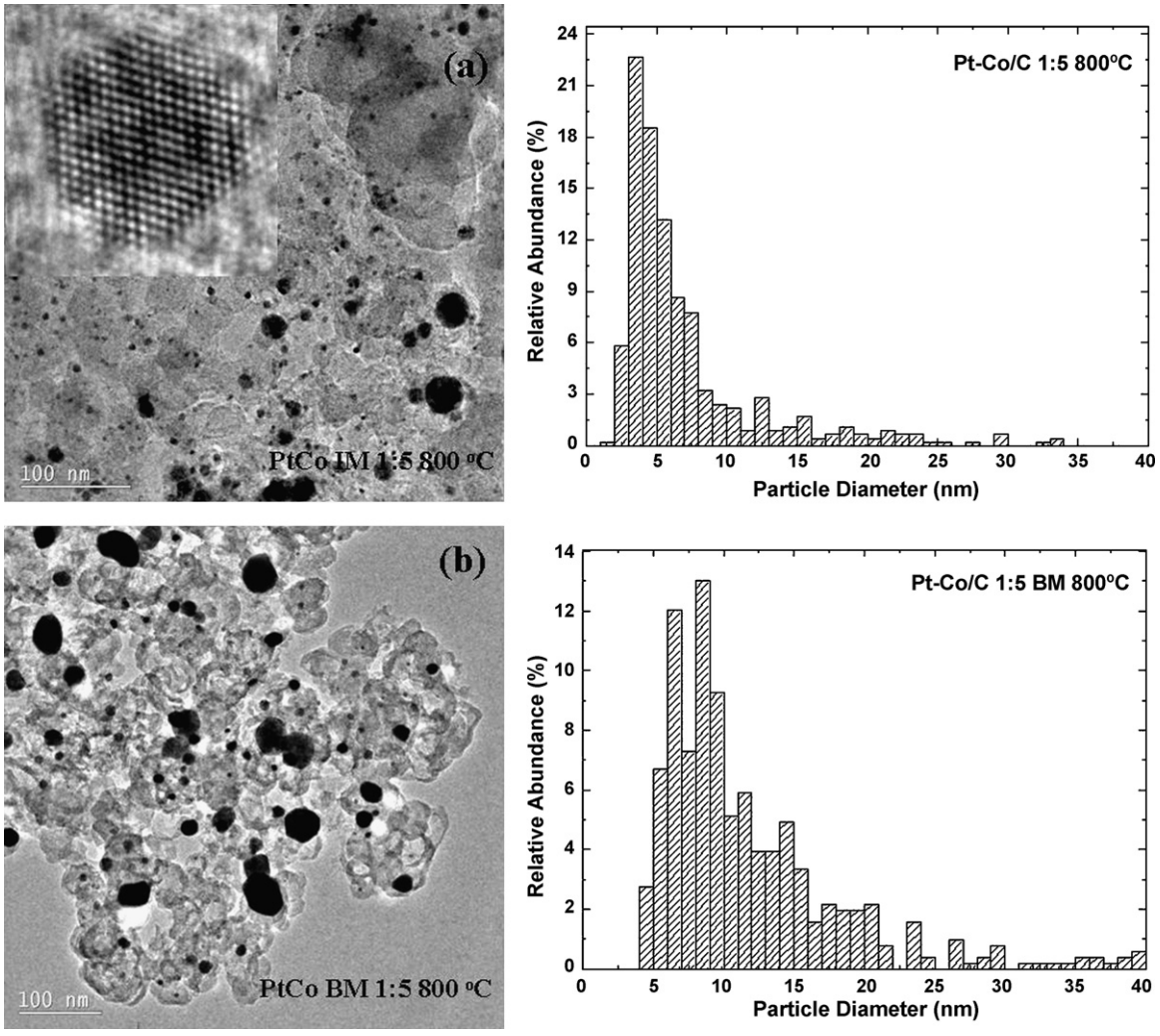

Fig. 2. TEM micrographs and particle size distribution histograms obtained from the micrographs Pt–Co/C 1:5 catalysts prepared by (a) Impregnation Method (IM), and (b) Borohydrid Method (BM), both treated at 800 °C, in hydrogen atmosphere.

reference electrode, but here, all potentials are quoted with respect to the reversible hydrogen electrode. The experiments were carried out in 1.0 mol L^{-1} KOH electrolyte, prepared from high purity reagent (Merck) and water distilled and purified in a Milli-Q (Millipore) system. The electrolyte was saturated with purified N_2 or O_2 gases, depending on the experiments. The electrochemical experiments were recorded in the range of potentials from 0.05 to 1.2 V using an AUTOLAB model potenciostat (PGSTAT30). Cyclic voltammograms were recorded at 0.10 V s^{-1} and stead state polarization curves were carried out point-by-point in several rotations rates to evaluate the ORR kinetics. All the experiments were conducted at room temperature (25 ± 1 °C).

The working electrodes for the electrochemical experiments were composed of the metal/C catalysts deposited as an ultra-thin layer over a pyrolitic graphite disk of a rotating disk electrode (RDE) (5 mm diameter, 0.196 cm^2). An aqueous suspension of 1.0 mg mL^{-1} of the metal/C was produced by dispersing the catalyst powder in pure water (Millipore) in an ultrasound system [5]. A 14 μL aliquot of the dispersed suspension was pipetted on the top of the pyrolitic carbon substrate surface and dried under vacuum, yielding a Pt loading of 14 μg cm^{-1}. After the evaporation of water, 20 μL of a diluted Nafion solution (prepared from a 5% solution, Aldrich) were pippeted onto the surface of the catalyst in order to attach the catalytic particles on the disk electrode substrate. Right after preparation, the electrodes were immersed into a N_2 saturated 1.0 mol L^{-1} KOH electrolyte.

3. Results and discussion

The effect of the thermal treatment on the particle size for the catalyst prepared by IM and BM was investigated by HRTEM measurements. Fig. 1a and b show representative HRTEM images for the Pt–Co/C 1:3 IM catalysts, treated at 500 and 800 °C, together with the obtained particle diameter distribution histograms. Fig.. 2 compares the HRTEM images and the histograms of the Pt–Co/C 1:5 catalysts prepared by IM and BM, and treated at 800 °C in H_2 atmosphere. Inset in Fig. 2a, is shown the Pt–Co/C 1:5 IM 800 °C HRTEM image of a particle with size of 5 nm, evidencing the (1 0 0) and (1 1 1) planes. The particle sizes and the diameter ranges of each investigated material are presented in Table 1. It is observed that the distribution of particle sizes becomes sharper as the temperature and the Co content in the catalyst increases. This effect may be associated to the reduction of higher amount of Co-oxide and/or Co salt to metallic Co, in which part of this associates with Pt, forming a Pt–Co phase, and the other fraction forming a segregated metallic Co phase on the surface of the Pt–Co/C particle.

The measurements for the Pt–Co/C 1:3 IM 500 °C (Table 1) showed a mean particle diameter of 8.6 nm with 1.0% of the particles presenting diameters above 37 nm, indicating a good particle spatial dispersion without the formation of large particle aggregates. Pt–Co/C 1:3 IM 800 °C has relatively small particles (mean diameter of 9.2 nm), and the size distribution histogram shows the existence of only 2% of the particles with diameter above 42 nm. The Pt–Co/C 1:5 IM 800 °C catalyst has smaller particles (mean diameter of 7.3 nm), and the size distribution histogram shows the existence of only 2% of the particles with diameters in the range of 32 nm to 34 nm. Compared to the Pt–Co/C 1:5 BM 800 °C (mean diameter 13.3 nm), it is seen that the IM presents higher efficiency for the formation of smaller particles. The Pt–Co/C 1:3 IM 200 °C catalyst has the largest particles (mean diameter 14 nm) and the broader size distribution, with 1% of the particles with *ca.* 35 nm and above. The HRTEM results together with experiments of temperature-programmed reduction (TPR) (not shown), indicate that, in this case, the Pt particles are covered by Co-oxide and/or the Co-salt, which were not reduced in the hydrogen atmosphere at this temperature. Thus, the measured diameter of the particles is counting this relatively thick layer, and that is the reason why the Pt–Co/C 1:3 IM 200 °C catalyst presents higher size than Pt–Co/C 1:3 IM 500 °C and Pt–Co/C 1:3 IM 800 °C, and also, why the HRTEM average particle diameter is larger than that obtained by XRD (see below).

Fig. 3 shows HRTEM images of the Pt–Co/C 1:5 IM 800 °C catalyst nanoparticles, before and after cycling the catalyst in a 0.5 mol L^{-1} H_2SO_4 solution. EDS measurements showed that the particle sub-

Table 1
Morphological information on the catalysts obtained by HRTEM: mean particle diameter with respective standard deviation, maximum measured diameter and diameter range of peak relative abundance.

Catalyst	Mean diameter (nm)	Standard deviation (±) (nm)	Maximum diameter (nm)
PtCo 1:3 IM 200 °C	14.0	6.5	34.3
PtCo 1:3 IM 500 °C	8.6	4.9	38.3
PtCo 1:3 IM 800 °C	9.2	5.8	43.0
PtCo 1:5 IM 800 °C	7.3	6.1	50.0
PtCo 1:5 BM 800 °C	13.3	9.6	76.9

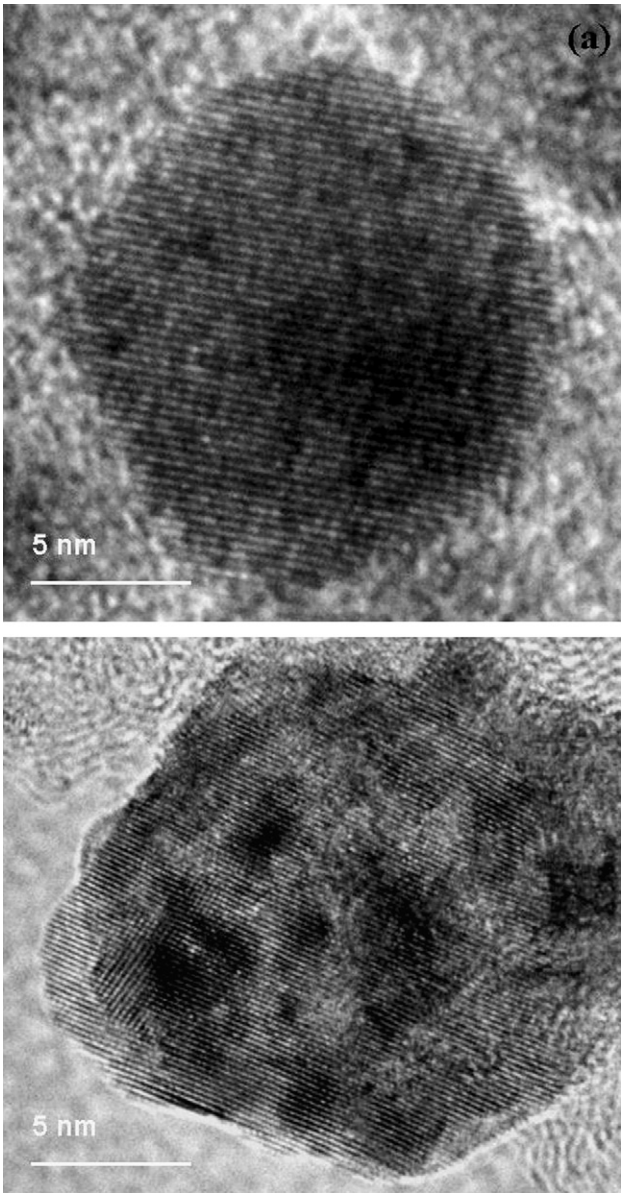

Fig. 3. TEM micrographs for nanoparticles of the Pt–Co/C 1:3 IM 800 °C electrocatalyst obtained before (a), and after cycling (b) in 0.5 mol L^{-1} H_2SO_4 solution.

mitted to the potential cycling in the acid solution was corroded mainly at the surface, mostly with Co dissolution. This phenomenon is further discussed below.

Fig. 4a and b show the X-ray diffraction patterns for the Pt/C and Pt–Co/C electrocatalysts synthesized by IM and BM, respectively. A broad reflection at $2\theta = 25^\circ$ observed in all cases is due to the carbon support. In the case of the Pt–Co/C catalysts prepared by IM, and thermally treated at 500 and 800 °C, it is clearly observed additional superlattice reflections such as the (1 1 0) and (1 0 0) reflections (Fig. 4a), indicating the formation of ordered PtCo type structures [20,21]. This evidences higher degree of alloying or higher platinum–cobalt interaction for the materials treated at higher temperatures. Also, in the Fig. 4a, it is noted that increasing the Co content (PtCo/C 1:3 to 1:5, prepared by IM) and the temperature of treatment, it is observed the growth of peaks related to a pure Co phase at *ca.* 44.2°, 51.6°, 75.8° and 91.8°, which indicates reduction of some Co-oxide phase, still remaining on the catalyst, to a segregated phase of metallic Co at the Pt–Co/C particle surface. For the catalysts prepared by BM, the XRD patterns (Fig. 4b) show only the five main characteristic peaks of the face-centered cubic (fcc) structure of crystalline Pt, namely the planes (1 1 1), (2 0 0), (2 2 0), (3 1 1) and (2 2 2). These five diffraction peaks are only slight shifted to higher angles with respect to those of the Pt/C electrocatalyst. This indicates a very low lattice contraction, evidencing low degree of alloy formation or low insertion of Co atoms into the Pt lattice. The increase of the temperature of thermal treatment caused only the growth of the Pt–Co particles and very low decrease in the lattice parameter. These two effects can be observed by the increase in the peak height and the constancy in 2θ of the diffraction peaks with the increase of the temperature. The major fraction of the Co atoms must be forming a segregated amorphous Co-oxide phase at the carbon support. The average crystallite sizes were calculated from the width of the half-height of the Pt (2 2 0) pattern using the Sherrer's equation [22]. These values are included in Fig. 4 for catalysts for which there is no diffraction peak overlaps. The results evidence an increase of the crystallite size with the increase of the temperature of treatment, in accordance with the HRTEM data. Also, there are no significant differences on the crystallite sizes, in most of the cases, for the materials with different compositions, for both routes of synthesis.

Since the Pt–Co/C catalysts prepared by IM showed higher degree of alloying, *in situ* XANES analyses were carried out to determine the electronic features of the Pt 5 d-band in these materials. Fig. 5 shows the *in situ* XANES results for the Pt–Co/C 1:3 IM catalysts thermally treated at (a) 500 °C and (b) 800 °C, compared to those for Pt/C E-TEK, obtained at 0.20 V and 0.90 V *vs.* RHE. The absorption at the Pt L_3 edge (11564 eV) corresponds to $2p_{3/2}$-5d electronic transitions and the magnitude of the absorption hump or white line located at *ca.* 5 eV from the edge is directly related to the Pt 5d electronic occupancy. The higher the hump the lower the occupancy and vice-versa. For all catalysts it is seen that the white line magnitude increases with the increase of the electrode potential. This phenomenon is attributed to the emptying of the Pt 5d-band, in agreement with the presence of an electron withdrawing effect of the oxygen present in a well-known surface oxide layer formed above 0.8 V on the catalyst particle surface [4].

In the Fig. 5a and b it is seen that at 0.20 V the magnitude of the white lines are somewhat higher for the Pt–Co/C materials, when compared to that for Pt/C. This evidences a higher vacancy of the Pt atoms, suggesting the occurrence of an electron withdrawing effect of Co on the Pt atoms. On the other hand, an important aspect observed is that the increase of the magnitude of the white line at 0.9 V, in relation to that at 0.2 V, is higher for the Pt/C than that for the Pt–Co/C materials. So, the change of the Pt 5 d vacancy, caused by oxide formation on the Pt atoms at 0.90 V is less pronounced for the Pt–Co/C materials, compared to Pt/C. This effect seems to

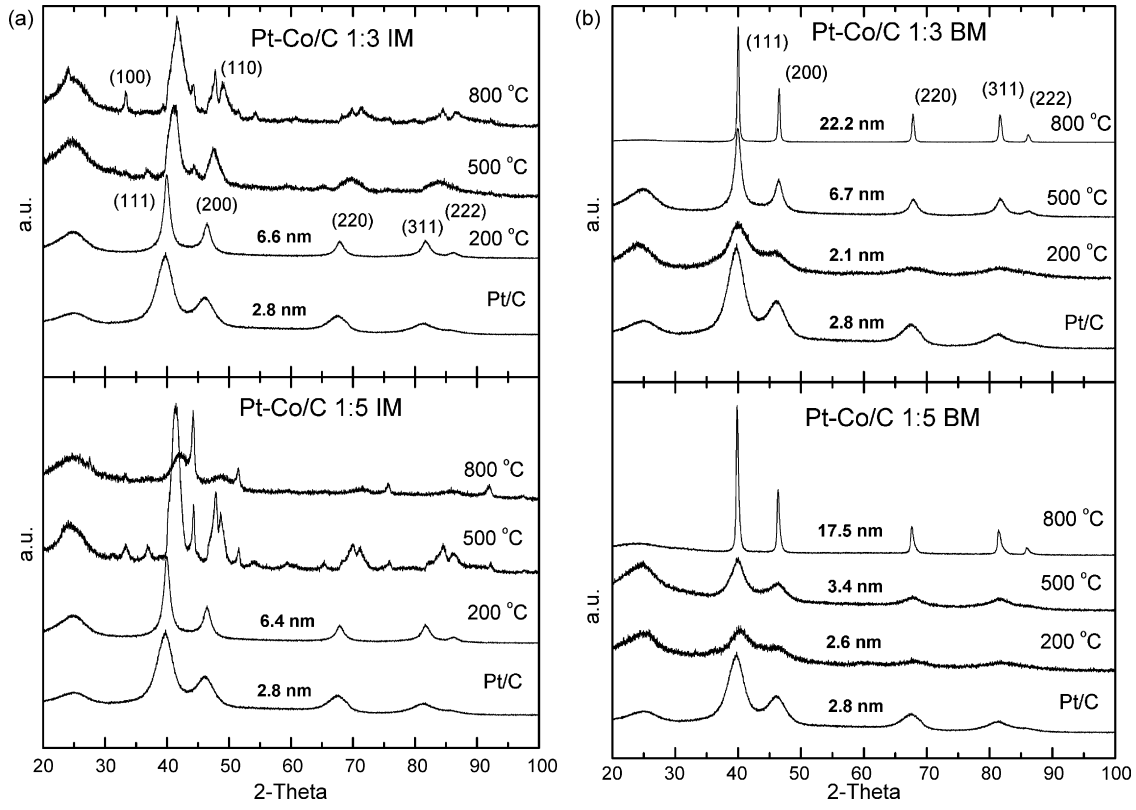

Fig. 4. X-ray diffraction (XRD) patterns for the Pt–Co/C electrocatalysts obtained for the materials treated at different temperatures in hydrogen atmosphere and prepared by (a) Borohydrid Method and (b) Impregnation Method. Numbers above the diffraction lines corresponds to the average crystallite sizes obtained using the Sherrer's equation [22].

be more evident for the materials treated at the higher temperature, evidencing higher electronic interaction of Pt and Co when the materials are treated at higher temperatures (higher degree of alloying).

The absorption magnitude of the Pt white line at 0.90 V is also dependent on the relative amount of Pt atoms in the particle surface, with respect to that in the bulk of the particle (the lower the particle size, the higher the percentage of atoms at the surface). That is due to the interaction of the Pt atoms at the surface of the particle with oxygen species formed above 0.80 V, due to the water activation [4]. The higher the amount of Pt atoms at the surface, the higher the number of Pt atoms with adsorbed oxygen species. So, the smaller enhancement of the Pt 5d white line observed at 0.90 V for the Pt–Co/C heat treated particles, compared to Pt/C, can be just a consequence of the higher size of the former catalyst particles (Table 1 and inset in Fig. 4), besides the fact that the surface is shared by both Pt and Co atoms. However, the smaller white line of Pt–Co/C compared to Pt/C can be also explained based on the withdrawing electron phenomenon of Co, which reduces the Pt density of states close to the Fermi level and so, leading to a lower Pt d-band center. This would reduce the adsorption strength of adsorbates as OH and/or O from the reaction intermediates and/or from the water activation on the Pt surface. Similar effects were already reported in a previous work [3] with PtV/C, PtCr/C and PtCo/C, (1:1 atomic ratios), and with varying Co contents in the catalyst particles [23].

Fig. 6 shows the cyclic voltammograms (CV) obtained for the Pt–Co/C catalysts prepared by BM (Fig. 6a) and by IM (Fig. 6b), with

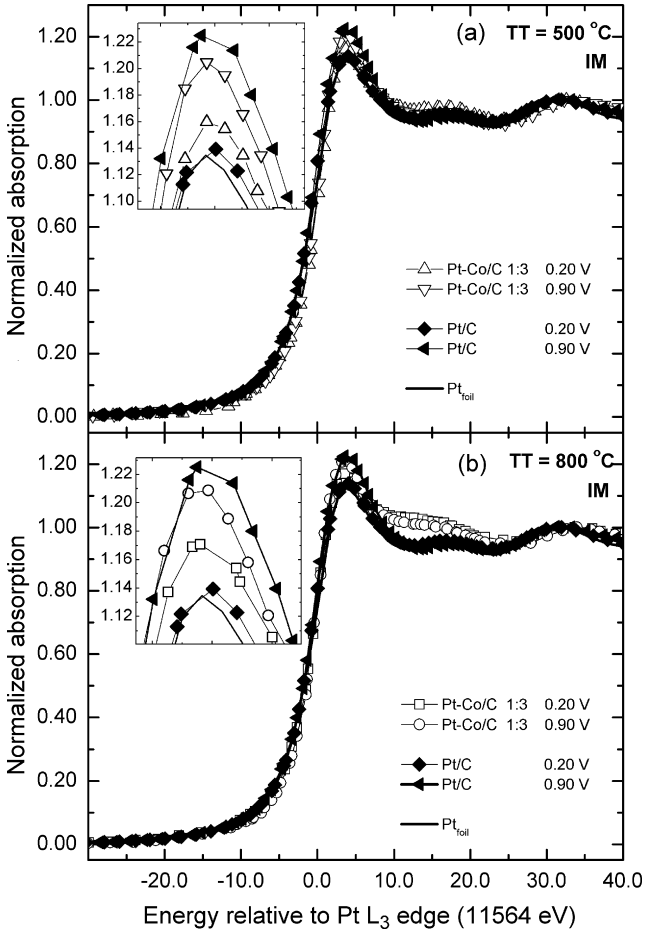

Fig. 5. *In situ* XANES spectra at the Pt L_3 edge for the Pt–Co/C 1:3 IM catalysts thermally treated at (a) 500 °C, and (b) 800 °C, compared to those obtained for Pt/C, at different electrode potentials in 1.0 mol L^{-1} KOH electrolyte. The *ex situ* spectrum obtained for a Pt foil is also included.

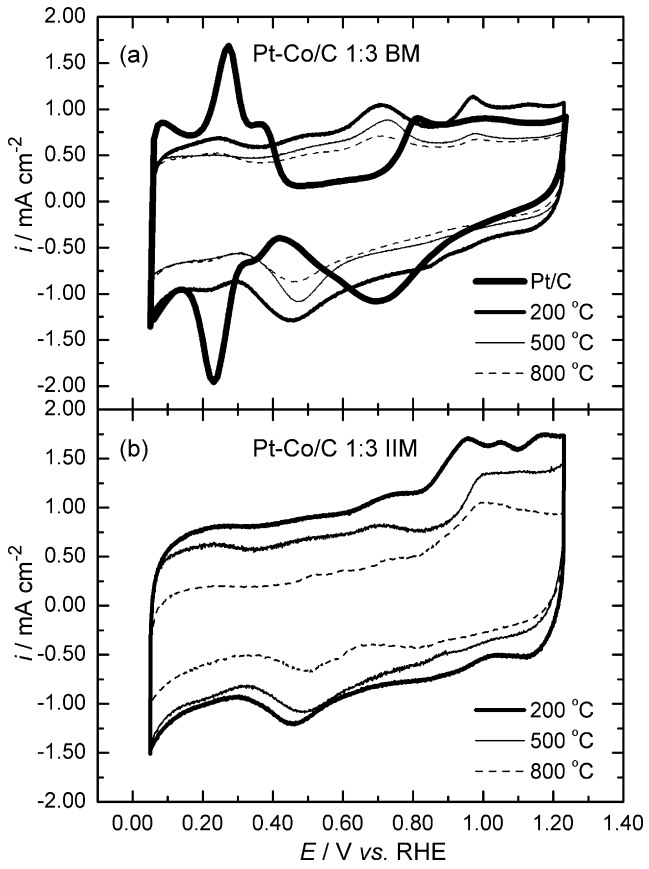

Fig. 6. Cyclic voltammograms for the Pt–Co/C 1:3 electrocatalysts in 1.0 mol L^{-1} KOH obtained for the materials treated at different temperatures in hydrogen atmosphere and prepared by (a) Borohydrid Method and (b) Impregnation Method. Scan rate of 0,1 V s^{-1}.

currents normalized per geometric area of the carbon disc substrate. The CV obtained for the commercial Pt/C E-TEK is included in Fig. 6a for comparison. The results show the typical behavior regarding the hydrogen and oxide regions for Pt/C [24,25]. In the case of the platinum–cobalt alloys, the presence of a redox pair located at around 0.4/0.7 V is noted, and this may be assigned to a redox process involving $Co(OH)_2/Co(OH)_3$ species in close contact to the surface Pt atoms. Above 0.9 V, anodic currents are observed for all Pt–Co/C materials, and this is ascribed to the formation of irreversible Co oxides. For all catalysts, a reduced charge corresponding to the hydrogen under-potential deposition (UPD) region of the CV is found, in comparison to pure Pt/C. This indicates a reduced Pt surface area or a reduced number of electrochemically active Pt atoms at the surface. Another observed effect is the decrease of the CV currents with the increase of the temperature of thermal treatment. This evidences an increase of the catalyst particle size due to the thermal treatment at higher temperatures, which promotes the metallic crystallite growth, as also shown by the XRD and HRTEM measurements, decreasing the total surface area. Also, from the CV results, it can be inferred that no Pt surface enrichment is achieved by increasing the temperature of thermal treatment. The CV profiles indicate that a considerable amount of Co atoms is present in the particle surface.

Steady state polarization curves for the ORR on the different electrocatalysts are shown in Fig. 7. Results for Pt/C and Co/C are included for comparisons. It is noted that the ORR limiting current densities assume close values for Pt/C and Pt–Co/C 1:3. This is in agreement with an ORR mechanism following mainly the four-electron pathway [24]. Lower values of limiting currents are observed for Pt–Co/C 1:5, which approach the values obtained for

Co/C. This evidences that, for this catalyst, the reaction takes place preponderantly at Co atoms at the particle surface and at the carbon support, and so, following a parallel route via two-electrons, as proposed before [26].

The comparison of the half-wave potentials in the polarization curves evidences that the catalytic activity of Pt/C is higher than those of the Pt–Co/C catalysts, even for thermally treated alloys. As observed above, the Pt surface enrichment was not achieved and so, a large amount of the non-noble metal atoms is present at the surface of the alloy particles. As the electrolyte is alkaline, the non-noble metal may be forming an oxide or hydroxide phase at the catalyst surface. This could introduce a "screening" effect [27] on neighboring Pt atoms lowering the number of Pt sites for the oxygen reduction reaction. The screening effect may overcome any electronic effect induced by the Co atoms, and this can explain the lower activity of the Pt–Co/C catalysts compared to Pt/C.

As the Pt surface enrichment on the Pt–Co/C catalysts was not reached by thermal treatment, the electrode composed by the Pt–Co/C 1:5 IM 800 °C alloy was submitted to a potential cycling in 0.5 mol L^{-1} H_2SO_4 electrolyte, with aim of dissolve some of the Co atoms present at the particle surface. The cycling was carried out at 300 mV s^{-1} in the range of 0.05 to 1.2 V *vs.* RHE, and a stable profile was observed after five cycles. Fig. 8 shows the CV curves obtained for Pt–Co/C 1:5 IM 800 °C in 1.0 mol L^{-1} KOH before and after cycling in the H_2SO_4 solution. The CVs for Co/C and Pt/C were included in Fig. 8a for comparison. After cycling in the acid electrolyte, the CV for the Pt–Co/C catalyst shows an increase of the double layer charge, and the peaks corresponding to the UPD of hydrogen was clearly observable, with the CV profile approximating to that of Pt/C. This indicates an increase of the catalyst surface area, and a Pt enrichment in the particle surface, due to the Co dissolution. So, after the potential cycling, the catalyst particles possess higher surface active area, and become composed by a Pt-rich shell, and a Pt–Co alloy core. This composition proposal is supported by the HRTEM results shown in Fig. 3, in which EDS measurements, conducted close to the edge of the particles, revealed a composition of 5:1 (Pt:Co) after submitting the catalyst to the cycling in the acid solution. The polarization curves for the O_2 reduction on the cycled Pt–Co/C 1:5 IM 800 °C catalyst and on Pt/C E-TEK are compared in Fig. 9. Here, the half-wave potentials of these curves clearly indicate higher activity for the cycled alloy catalyst.

The higher activity obtained for the cycled Pt–Co/C 1:5 IM 800 °C catalyst, after the Co dissolution from the particle surface, seems to be, mainly, a consequence from its higher surface area. Similar approach was investigated in Ref. [28]. Furthermore, its higher activity, possibly, has some contribution from the lower "screening effect", and of a modification in the 5d-band properties of the surface Pt atoms, mainly caused by lattice mismatch and/or by a strong electronic coupling of the Pt in the shell and Co atoms in the beneath layer. A lattice mismatch of the Pt atoms on the Pt-rich surface and the Pt–Co alloy core may exist, caused by the Pt–Pt bond contraction due to the presence of the Co atoms, which have atomic radii lower than that of Pt. However, this may conduct to a small compressive strain in the Pt surface layer and, probably, this effect contributes little to the changes on the Pt 5d-band properties. On the other hand, the electronic interaction of the Pt and Co atoms (ligand effect) leads to a significant lowering of the Pt d-band center [8]. This effect conducts to a faster electro-reduction of oxygenated intermediates and/or a decrease on the Pt-oxides coverage from water activation, in both cases inducing an increase of the ORR kinetics. So, the role of Co atoms is, principally, to promote the increase of the catalyst surface area, after their leaching from the surface, and to lower the Pt d-band center, as a result of the electronic interaction of the Pt atoms at the catalyst surface, and the Co atoms in the inner layer.

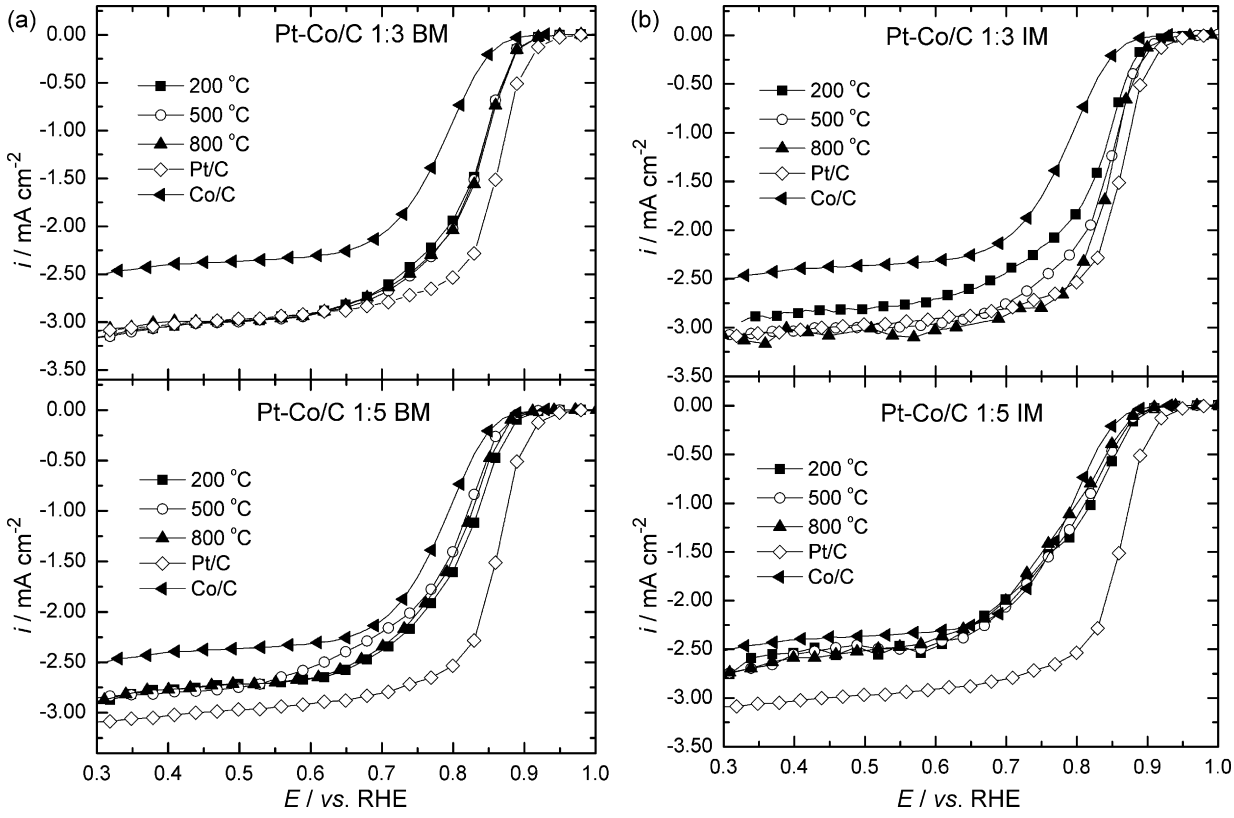

Fig. 7. Steady-state polarization curves for the Pt–Co/C electrocatalysts in 1.0 mol L^{-1} KOH obtained for the materials at different atomic ratios and thermally treated at different temperatures in hydrogen atmosphere, and prepared by (a) Borohydrid Method and (b) Impregnation Method. Rotation rate of 1600 rpm.

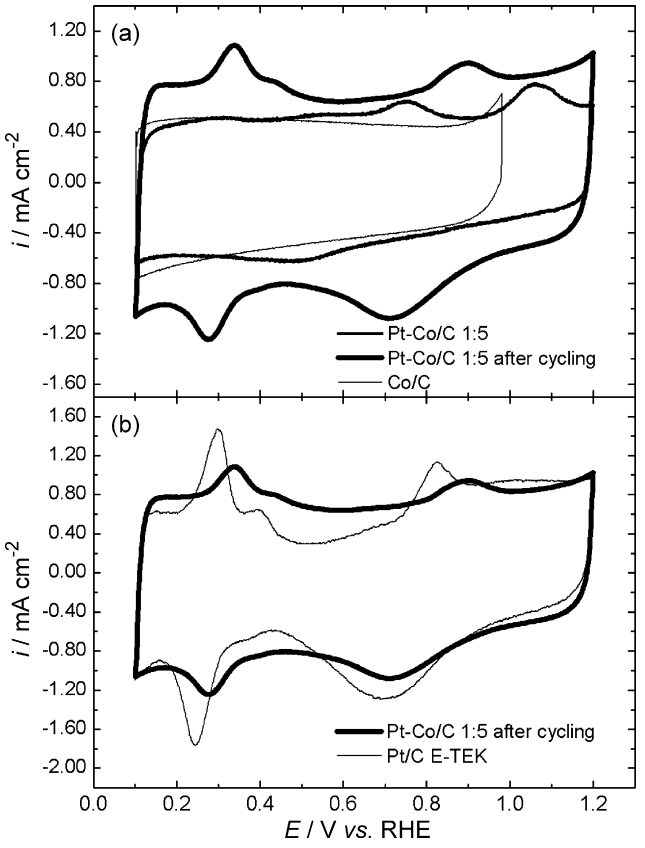

Fig. 8. Cyclic voltammograms, for the Pt–Co/C 1:3 IM 800 °C electrocatalyst in 1.0 mol L^{-1} KOH obtained before and after cycling the material in 0.5 mol L^{-1} H_2SO_4 solution (a), and comparison with Pt/C (b). The cyclic voltammogram obtained for the Co/C material is included in (a) for comparison. Scan rate of 0.1 V s^{-1}.

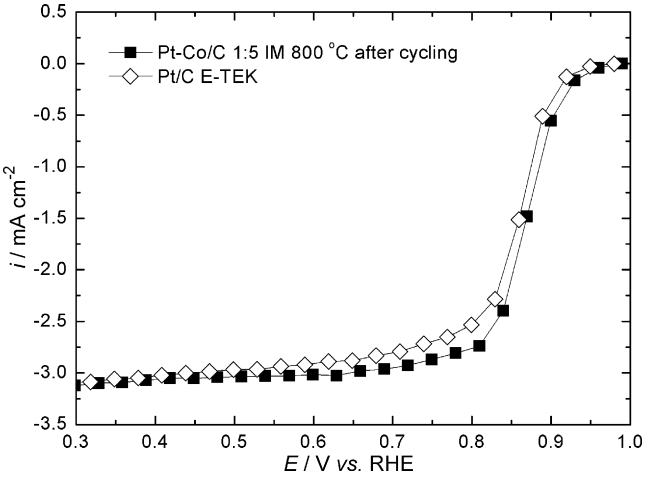

Fig. 9. Polarization curves for the Pt–Co/C 1:3 IM 800 °C electrocatalyst in 1.0 mol L^{-1} KOH obtained before and after cycling the material in 0.5 mol L^{-1} H_2SO_4 solution.

4. Conclusions

HRTEM images showed that the distribution of the catalyst particle sizes becomes sharper as the temperature of thermal treatment and the Co content in the catalyst particles increase. *In situ* XANES measurements indicated smaller Pt-oxide formation on Pt–Co/C compared to Pt/C, and this was explained based on the withdrawing electron phenomenon of Co, lowering the Pt d-band center. Polarization results indicated a higher electrocatalytic activity of Pt/C compared to the Pt–Co/C materials. This was attributed to the presence of oxides groups attached on the non-noble metal at the particle surface, which introduces a "screening effect" on neighboring Pt atoms, decreasing the number of active sites for the ORR. The higher activity of the Pt–Co/C material, submitted to the potential cycling in acid electrolyte, was ascribed, mainly, to its higher surface area, obtained as a result of the Co leaching from the particle surface. Also, its higher activity was attributed to a minor contribution from the lower "screening effect", and to the Pt electronic coupling with the Co atoms located in the beneath layer of the surface Pt atoms, decreasing the Pt 5d-band center. This conducts to a weaker Pt–OH bond strength, increasing the ORR kinetics due to a faster electro-reduction of the oxygenated intermediates and/or a decreased Pt-oxides coverage that arises from the water activation at higher electrode potentials.

Acknowledgments

The authors thank the Fundação de Amparo à Pesquisa do Estado de São Paulo (FAPESP), the Conselho Nacional de Desenvolvimento Científico e Tecnológico (CNPq) for financial assistance, and the Brazilian Synchrotron Light Source Laboratory (LNLS), Brazil, for assisting with the HRTEM and XAS experiments.

References

[1] J. Zhang, Y. Mo, M.B. Vukimirovic, R. Klie, K. Sasaki, R.R. Adzic, J. Phys. Chem. B 108 (2004) 10955.
[2] U.A. Paulus, A. Wokaun, G.G. Sherer, T.J. Shmidt, V. Stamenkovic, V. Radmilovic, N.M. Markovich, P.N. Ross, J. Phys. Chem. B 106 (2002) 4181.
[3] F.H.B. Lima, M.J. Giz, E.A. Ticianelli, J. Braz. Chem. Soc. 16 (2005) 328.
[4] S. Mukerjee, S. Srinivasan, M.P. Soriaga, J. McBreen, J. Electrochem. Soc. 142 (1995) 1409.
[5] M. Min, J. Cho, K. Cho, H. Kim, Electrochim. Acta 45 (2000) 4211.
[6] A.S. Arico, A.K. Shukla, H. Kim, S. Park, M. Min, V. Antonucci, Appl. Surf. Sci. 172 (2001) 33.
[7] B. Hammer, J.K. Nørskov, Surf. Sci. 343 (1995) 211.
[8] J.R. Kitchin, J.K. Nørskov, M.A. Barteau, G. Chen, J. Chem Phys. 120 (2004) 10240.
[9] B. Hammer, J.K. Nørskov, Adv. Catal. 45 (2000) 71.
[10] J. Greeley, J.K. Nørskov, M. Mavrikakis, Annu. Rev. Phys. Chem. 53 (2002) 319.
[11] V. Stamenkovic, B.S. Mun, K.J.J. Mayrhofer, P.N. Ross, N.M. Markovic, J. Rossmeisl, J. Greeley, J.K. Nørskov, Angew. Chem. Int. Ed. 45 (2006) 2897.
[12] J. Zhang, M.B. Vukmirovic, Y. Xu, M. Mavrikakis, R.R. Adzic, Angew. Chem. Int. Ed. 44 (2005) 2132.
[13] L. Xiong, A.M. Kannan, A. Manthiram, Electrochem. Commun. 4 (2002) 898.
[14] Y. Kiros, J. Electrochem. Soc. 143 (1996) 2152.
[15] J. McBreen, W.E. O'Grady, K.I. Pandya, R.W. Roffman, D.E. Sayers, Langumuir 3 (1987) 428.
[16] H. Tolentino, J.C. Cezar, D.Z. Cruz, V. Compagnon-Caillol, E. Tamura, M.C. Alves, J. Synchrotron. Radiat. 5 (1998) 521.
[17] T. Ressler, J. Phys. IV C2 (7) (1997) 269.
[18] K.I. Pandya, R.W. Roffman, J. McBreen, W.E. O'Grady, J. Electrochem. Soc. 137 (1990) 383.
[19] J.B.A.C. van Zon, D.C. Konigsberger, H.F.J. Van't Blik, D.E. Sayers, J. Chem. Phys. 82 (1985) 5742.
[20] L. Xiong, A. Manthiram, J. Electrochem. Soc. 152 (2005) 697.
[21] JCPDS—Joint Committee on Powder Diffraction Standards, International Center for Diffraction Data (ICDD), Newton Square, PA 19-073, USA, 1980.
[22] A.R. West, Solid State Chemistry and Its Applications, Wiley, New York, 1984, 180.
[23] F.H.B. Lima, J.R.C. Salgado, E.R. Gonzalez, E.A. Ticianelli, J. Electrochem. Soc. 154 (2007) A369.
[24] J. Perez, E.R. Gonzalez, E.A. Ticianelli, Electrochim. Acta 44 (1998) 1329.
[25] F.H.B. Lima, E.A. Ticianelli, Electrochim. Acta 49 (2004) 4091.
[26] F.H.B. Lima, J.F.R. de Castro, E.A. Ticianelli, J. Power Sources 161 (2006) 806.
[27] M.D. Obradovic, B.N. Grgur, Lj.M. Vracar, J. Electroanal. Chem. 548 (2003) 69.
[28] P. Mani, R. Srivastava, P. Strasser, J. Phys. Chem. C 112 (7) (2008) 2770.